SAR Image Despeckling Based on Lapped Transform Domain Dual Local Wiener Filtering Framework

Deepika Hazarika, *Member, IAENG* Vijay Kumar Nath, *Member, IAENG* and Manabendra Bhuyan

Abstract—**In this paper, a Synthetic Aperture Radar (SAR) image despeckling technique, based on lapped orthogonal transform (LOT) domain dual local Wiener filtering framework, is proposed. A logarithmic transformation is employed to convert the speckle contribution into additive noise. It is demonstrated that the local distribution of dyadic rearranged LOT coefficients of logarithmically transformed SAR images are well approximated using Gaussian distribution. The proposed LT domain structure employs two local Wiener filtering procedures to despeckle the SAR images. The signal variance is estimated using elliptic directional windows for different oriented subbands. The motivation of using lapped transform (LT) is that they are robust to oversmoothing and preserve better oscillatory image components like textures. Experiments on real SAR images, show that the proposed method reduces speckle noise effectively while preserving textures and outperforms well known iterative probabilistic patch-based (PPB) filter and a recent directionlet based method, with much less computational complexity.**

Index Terms—**Lapped orthogonal transform, Speckle reduction, Synthetic aperture radar images, Dual local Wiener filtering, Elliptic directional window.**

I. INTRODUCTION

SAR images provide important information in many applications like surface surveillance, mine detection, automatic target recognition, search and rescue etc. The main problem in SAR imagery is that textures are usually corrupted by multiplicative speckle noise which is due to the coherent radiation in the process of imaging. The texture in the images usually contains very important information about the scene. The presence of speckle badly affects the human interpretation and further analysis. Thus, the despeckling of SAR images while preserving textural information is highly important.

A number of spatial domain methods have been proposed in the literature. The earlier spatial filters like Lee [1], Frost [2], Kuan [3] and Gamma MAP filter[4] work directly on intensity image and exploits the local statistics. These spatial filters often reduce the speckle at the cost of oversmoothing the details of the image. The SRAD (speckle reducing anisotropic diffusion) filter [5] is very effective in terms of speckle noise reduction and detail preservation compared to earlier spatial domain methods. In the well known probabilistic patch based (PPB) algorithm [6], the authors proposed a weighted maximum likelihood denoising method with probabilistic patch-based weights. The weights

are iteratively refined based on the similarity between the noisy patches and the similarity of patches obtained from the previous estimate. The PPB algorithm have shown excellent despeckling results in the literature but its computational complexity is very high. The iterative version of PPB filter generally shows better despeckling performance only in low signal to noise ratio images.

In last one and half decades, the discrete wavelet transforms (DWT) have been universally recognized as extremely strong tool in image processing [7], [8], [9], [10], [11], [12], [13], [14] and have been used with good success in reducing speckle noise from SAR images[15], [16], [17]. The DWT based speckle reduction techniques overcome the problem of earlier spatial domain techniques[15], [18], [16], [19], [17] and are implemented in homomorphic and non-homomorphic frameworks. In the popular homomorphic [20] based approach, the logarithm operator is applied on the noisy image to convert the multiplicative noise into additive one. In [21] Solbo et al., in non-homomorphic framework, proposed a wavelet domain Γ-WMAP (wavelet maximum a posteriori) filter. This filter exhibits high amount of blurring and oversmooth textures present in the images. Solbo et al. in [19] introduced an improved wavelet domain homomorphic Γ-WMAP filter. The authors proposed to use the normal inverse Gaussian (NIG) distribution as a statistical model for the wavelet coefficients of both the reflectance image and the noisy image. A MAP estimator using the symmetric α-stable pdf was employed for the estimation of noise free wavelet coefficients [16]. It was shown that the wavelet coefficients of log transformed SAR images can be well modeled using α-stable distribution. Bhuiyan et al. [17] modeled the wavelet coefficients of log transformed SAR images using Cauchy pdf. A Bayesian minimum mean absolute error estimator and MAP estimator were employed using this prior to reduce the speckle from SAR images. In [22], a MAP estimator using 2D GARCH prior is used to estimate the noise free wavelet coefficients. The authors show that the wavelet coefficients of log transformed SAR images are best modeled using 2D GARCH model.

A number of non-homomorphic wavelet domain methods for speckle noise reduction also exist in literature. A low complexity mean based smoothing operation was employed in stationary wavelet transform (SWT) domain to despeckle the SAR images. The authors in [23] proposed a denoising method in undecimated wavelet domain using MAP estimator and assumed the pdf of each wavelet coefficient as Generalized Gaussian. The parameters of the Generalized Gaussian pdf are taken to be space varying within each wavelet frame. Argenti et al. in [24], show that the MAP

(a)   (b)   (c)

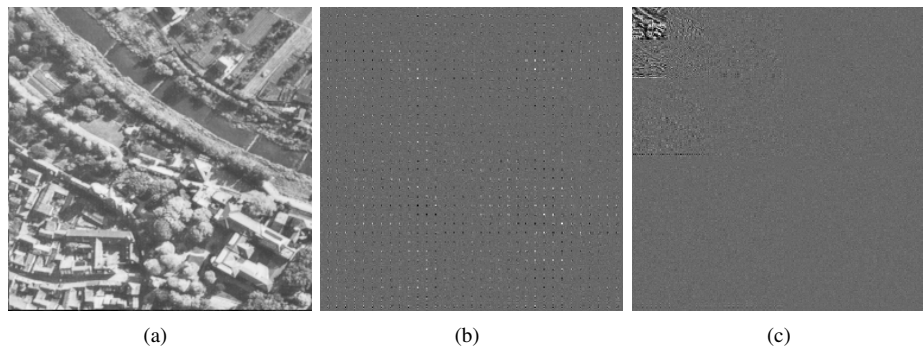Fig. 1. Rearrangement of block LOT (M=8) coefficients into 3 level wavelet like structure (a) Original aerial image (b) LOT block decomposition (M=8) (c) 3 level wavelet like structure (octave-like representation)

estimator in undecimated wavelet domain with coefficients modeled as Laplacian with Gaussian noise shows comparable despeckling results with the performance of MAP estimator in the same domain with the coefficients modeled as Generalized Gaussian, with computational complexity less than ten times. Parrilli et al. [25] introduced an improved form of BM3D method where several steps of original BM3D structure were modified to take care of SAR class of images.

The orthogonal DWT's are not very good in capturing the 2D singularities found in the images[26], [27], [28], [29]. To overcome this problem, various computationally complex transforms like directionlet, contourlet, bandelet, curvelet etc. have been proposed in the literature [26], [27], [28]. Recently, a few approaches on LT based image denoising have been proposed [30], [31], [32], [29]. The motivation for image denoising in LT domain is that LTs have good energy compaction and are robust to oversmoothing. The LTs are orthogonal transforms, hence signal and noise statistics can be modeled precisely in the LT domain. Since the LTs are block transforms, the LT coefficients are first rearranged in a wavelet like structure (octave like representation), then the subband statistics of the rearranged LT coefficients are modeled in a way similar to wavelet coefficients [30], [33], [29]. It has been shown that LT domain image denoising methods are very good in preserving oscillatory components present in the images like textures and shows competitive performance compared to wavelet domain techniques. The authors in [34], observed that the LOT based despeckling approaches are well capable in reducing the speckle noise from homogeneous regions and also preserves more textures. The LT has been proposed to overcome the annoying blocking artifact problem of DCT with increased coding gain and have extended basis functions which overlap across the block boundaries. The LTs are based on discrete cosine transform (DCT) for which fast implementation algorithms are available. The LOT can be efficiently computed using the flowgraphs discussed in Ref. [35]. Malvar [36] also demonstrated that the LOT has much lower computational complexity as compared to the fastest possible implementation of the "9/7" DWT via lifting.

Among the various approaches in wavelet based image denoising schemes, one popular class of approach is to use the linear minimum mean square error estimator(LMMSE) [37], [38], [39], [40], [41], [42], [43] to restore the noisy wavelet image coefficients. These methods assume the local distribution of the wavelet coefficients to be Gaussian with spatially varying variance. These methods are popular due to their good denoising performance and low computational complexity. In this paper, we introduce a dual local Wiener filtering framework in LOT domain to reduce speckle noise from SAR images assuming the local distribution of the log transformed LOT coefficients to be Gaussian with spatially varying variance.

This paper is organized as follows. In Section II, an introduction on LOT and statistical modeling of SAR image is presented. The proposed LT based despeckling framework is explained in Section III. In Section IV, the performance of proposed technique is evaluated and is compared with several SAR image despeckling methods. Finally, in Section V we give some conclusions.

II. LAPPED ORTHOGONAL TRANSFORM (LOT) AND STATISTICAL MODELING OF SAR IMAGE

A. LOT

The lapped orthogonal transform (LOT) [35], [44] is a block transform and was introduced as an alternative to 2D DCT with significantly reduced blocking artifacts. The basis functions of LOT are larger than the block size and decay smoothly to zero at the block boundaries which leads to highly reduced blocking artifacts. The LOT bases have length of $2M$ for a block of M sample.The *feasible* LOT matrix P which may not be necessarily optimal is computed from [44]

$$P = \frac{1}{2} \begin{pmatrix} D_e - D_o & D_e - D_o \\ J(D_e - D_o) & -J(D_e - D_o) \end{pmatrix} \qquad (1)$$

where D_e and D_o are the $MxM/2$ matrices containing the even and odd DCT functions respectively. The matrix J is the counter identity matrix

$$J = \begin{pmatrix} 0 & 0 & .... & 0 & 1 \\ 0 & 0 & .... & 1 & 0 \\ . & & . & & . \\ . & & . & & . \\ 0 & 1 & .... & 0 & 0 \\ 1 & 0 & ... & 0 & 0 \end{pmatrix} \qquad (2)$$

The optimal LOT matrix is computed by [35]

$$P_0 = PZ \qquad (3)$$

where Z is an orthogonal matrix. An optimal Z is required to obtain an optimal LOT matrix. The covariance matrix is given by [35]

$$R_0 = Z'P'R_{xx}PZ \qquad (4)$$

With P and R_{xx} fixed, the transform coding gain is maximized when R_0 is diagonal which signifies that the columns of Z are the eigen vectors of $P'R_{xx}P$. With such matrix Z, the optimal LOT matrix P_0 can be computed.

Xiong et al. in [45] introduced an octave-like representation for 8x8 block DCT coefficients and show that the 8x8 DCT coefficients can be rearranged into a single three level wavelet like structure. Malvar proposed a similar dyadic rearrangement for LT coefficients in [36] i.e. block LT coefficients can be rearranged into a wavelet-like structure of $J_w = \log_2 M$ decomposition levels. Fig. 1(b) shows block LOT decomposition (M=8) of a noiseless aerial image (Fig. 1(a)). Fig. 1(c) shows the rearrangement of LOT coefficients into 3-level wavelet like structure.

B. Speckle noise statistics

The model of SAR image has the following form (assuming the speckle to be fully developed)[46]

$$Z_{SAR}(i,j) = Y_{SAR}(i,j)\eta_{SAR}(i,j) \qquad (5)$$

where $Y_{SAR}(i,j)$ is a clean image, $Z_{SAR}(i,j)$ is the noisy observation of $Y_{SAR}(i,j)$. The $\eta_{SAR}(i,j)$ is the multiplicative noise component. The speckle considered here is a complex process with Gaussian distributed real and imaginary parts. The intensity of the resulting complex field is exponentially distributed and the amplitude is Rayleigh distributed [47]. In case of a L-look processing, the averaging of L independent observations is performed. The η_{SAR} is then modeled using a $\Gamma(L,L)$ distribution

$$P(\eta_{SAR}) = \frac{L^L \eta_{SAR}^{L-1} e^{-\eta_{SAR}L}}{\Gamma(L)} \qquad (6)$$

The logarithmic function is applied on both sides of (5) to convert the multiplicative noise model to an additive one.

$$\log Z_{SAR}(i,j) = \log Y_{SAR}(i,j) + \log \eta_{SAR}(i,j) \qquad (7)$$

(7) can be expressed as

$$Z(i,j) = Y(i,j) + N(i,j) \qquad (8)$$

where $Z(i,j), Y(i,j)$ and $N(i,j)$ are the logarithms of $Z_{SAR}(i,j), Y_{SAR}(i,j)$ and $\eta_{SAR}(i,j)$ respectively. The distribution of log transformed speckle can be well approximated by Gaussian distribution [17], therefore we assume log-transformed speckle noise to be additive white Gaussian noise with standard deviation σ_n.

C. Statistical Modeling of log transformed SAR image LOT coefficients

After applying the LOT on (8) and rearranging the block LOT coefficients into J level wavelet like structure (octave-like representation), we have

$$z_q^p(i,j) = y_q^p(i,j) + n_q^p(i,j) \qquad (9)$$

where $z_q^p(i,j)$, $y_q^p(i,j)$ and $n_q^p(i,j)$ represent the $(i,j)^{th}$ LOT coefficient, at orientation p with level q of the log transformed SAR image, the corresponding log transformed reflectance and the corresponding speckle component respectively. It is to be noted that due to orthogonality of the LOT, n is also independent identically distributed white Gaussian
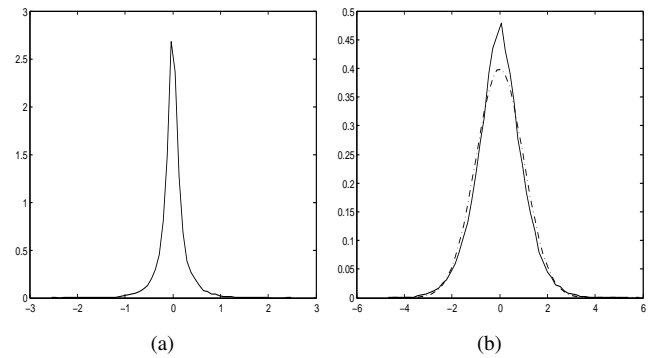

Fig. 2. (a) Histogram of one of the finest subbands of 'chinalake' SAR image (approximately noise free) (b) Solid line: Histogram of the same set of coefficients scaled by estimated local standard deviations, Dashed dotted line: Unit variance, zero mean Gaussian probability density function (Image Courtesy of Sandia National Laboratories, Airborne ISR)
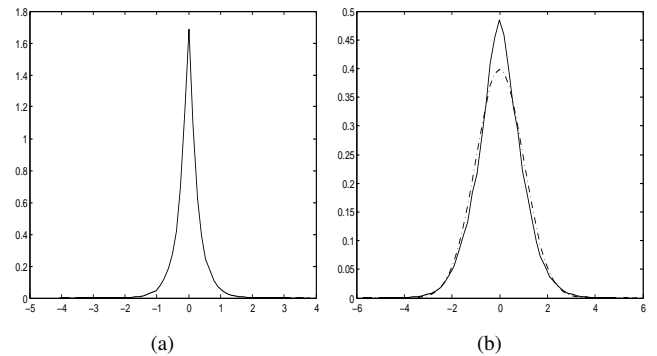

Fig. 3. (a) Histogram of one of the finest subbands of 'maricopa' SAR image (approximately noise free) (b) Solid line: Histogram of the same set of coefficients scaled by estimated local standard deviations, Dashed dotted line: Unit variance, zero mean Gaussian probability density function (Image Courtesy of Sandia National Laboratories, Airborne ISR)

with zero mean and standard deviation of σ_n. The mean value of the log-transformed speckle noise is biased and therefore requires a correction to adjust the bias so that the radiometric distortion can be avoided [48]. Hazarika et al. [34] study the global statistics of dyadic rearranged LOT coefficients of log transformed SAR images and show that the global statistics of subband coefficients is highly non Gaussian.

In this paper, we model the local distribution of the dyadic rearranged LOT coefficients of log transformed SAR image, to be independent and identically distributed Gaussian with zero mean and spatially varying variance. In order to justify the assumption of local distribution of the log transformed LOT coefficients to be Gaussian for SAR class of images, in Table I we determine the average skewness and kurtosis values for different subbands of dyadic rearranged LOT coefficients for three log transformed SAR (approximately clean) images, using 3x3, 5x5 and 7x7 square shaped neighborhoods (for the sake of simplicity). In Table I, for every neighborhood, the first and second rows show the corresponding average kurtosis and skewness values respectively. Since, all real SAR images are inherently contaminated by speckle noise, the real SAR images are first filtered using the well known PPB filter [6] and then the filtered images are treated as reasonable approximation of speckle free radar reflectivity. For a Gaussian distribution, the skewness value (which indicates about the symmetry of the distribution) is 0 and the kurtosis value (which indicates about the peakedness)

TABLE I
AVERAGE SKEWNESS AND KURTOSIS VALUES FOR DIFFERENT SUBBANDS OF DYADIC REARRANGED LOT COEFFICIENTS (M=8) FOR THREE LOG TRANSFORMED SAR (APPROXIMATELY CLEAN) IMAGES.(IMAGE COURTESY OF SANDIA NATIONAL LABORATORIES, AIRBORNE ISR)

Image	Neighborhood	Subbands								
		LH1	HL1	HH1	LH2	HL2	HH2	LH3	HL3	HH3
'airport'	3x3	2.659	2.758	2.550	2.532	2.601	2.546	2.622	2.628	2.603
		0.014	0.009	-0.001	-0.105	-0.105	0.031	0.011	0.063	-0.029
	5x5	3.867	4.177	3.553	3.306	3.584	3.358	3.862	3.947	3.553
		0.027	0.009	0.003	-0.144	-0.169	0.059	0.031	0.134	-0.056
	7x7	4.672	5.194	4.313	3.811	4.318	3.864	4.547	4.877	4.109
		0.038	0.005	0.005	-0.173	-0.204	0.067	0.013	0.213	-0.052
'maricopa'	3x3	2.545	2.559	2.515	2.667	2.668	2.579	2.654	2.642	2.808
		0.011	0.005	0.013	-0.066	-0.078	-0.005	0.010	-0.069	0.022
	5x5	3.456	3.535	3.453	3.901	3.861	3.603	4.319	4.279	4.239
		0.020	-0.006	0.021	-0.096	-0.117	0.007	0.052	-0.057	0.028
	7x7	4.056	4.223	4.143	4.969	4.958	4.337	5.935	5.778	5.239
		0.021	-0.016	0.024	-0.1177	-0.136	0.034	0.0716	-0.012	0.054
'piperiver'	3x3	2.723	2.744	2.606	2.644	2.656	2.668	2.855	2.888	2.889
		0.031	0.019	0.001	-0.114	-0.119	-0.022	0.046	0.069	-0.017
	5x5	4.085	4.151	3.859	3.795	3.787	3.947	4.896	4.786	4.719
		0.052	0.041	0.006	-0.126	-0.144	-0.042	0.164	0.109	-0.072
	7x7	5.132	5.244	4.926	4.828	4.759	5.004	7.171	6.505	6.384
		0.048	0.040	0.003	-0.114	-0.166	-0.059	0.336	0.089	-0.059

is 3. It can be observed from Table I that the skewness and kurtosis values are well close to zero and three respectively in most of the subbands. Therefore, Gaussian distribution is well able to model the local distribution of the dyadic rearranged LOT coefficients of log transformed SAR images. It is to be noted that the local Wiener filter provides optimal performance when both the signal and noise are Gaussian distributed[49]. Fig. 2(a) and Fig. 3(a) shows the histogram of one of the finest subband of 'chinalake' and 'maricopa' SAR images (approximately noise free) respectively. Fig. 2(b) and Fig. 3(b) shows the same coefficients when normalized by their estimated standard deviations respectively. It is observed that the normalized histogram is well approximated by a zero mean, unit variance Gaussian probability density function.

III. LOT BASED DUAL LOCAL WIENER FILTERING STRUCTURE FOR SAR IMAGE DESPECKLING

The local Wiener filtering in LOT domain can be performed in two major steps:

First the signal variance estimation for each coefficient in the LOT domain is carried out using the observed noisy coefficients in a local neighborhood. When the size of the region used for signal variance estimation is large and if the coefficients are locally independent and identically distributed, then the signal variance estimation is likely to be more reliable. But the locally independent and identically distributed assumption seems to be unreliable if we go on increasing the size of the neighborhood, which indicates that the reliable signal variance estimation can be achieved by choosing appropriate neighborhood region. Various techniques based on locally varying windows have been reported in the literature. In [50], the authors proposed the concept of adaptive window based variance estimation using the bootstrap technique. A square shaped window using region expansion was discussed in [51]. Eom and Kim [40] introduced a nearly arbitrarily shaped window to obtain more accurate local variance. Shui in [41] proposed elliptic directional windows, for different oriented subbands, for more reliable signal variance estimation. The elliptic directional window provides better estimates within and around energy clusters which helps in better preservation of edges and textures in the images[41].

We estimate the signal variances in each oriented subband using elliptic directional windows. The elliptic directional windows produces better variance estimates than simple square shaped windows [41]. For each noisy LOT coefficient, the signal variance is estimated by:

$$\hat{\sigma}_y^2(m,n) = \max\left(0, \frac{1}{W_{LD}} \sum_{(i,j)} z^2(m+i, n+j) - \sigma_n^2\right) \quad (10)$$

An elliptic directional window is expressed as [41]

$$W_{LD}(s_i, s_h) = \left\{(u,v) \in D^2 : u^2 + s_h^4 v^2 \leq s_h^2 s_i^2\right\} \quad (11)$$

where the parameters s_i and s_h are positive real numbers. The parameter s_i denotes the size of the window and s_h determines its shape. As the three oriented subbands usually show different directional features, we use a longer elliptic window $W_{LD}(s_i, s_h)(s_h > 1)$ in horizontal subbands and a higher elliptic window $W_{LD}(s_i, 1/s_h)(s_h > 1)$ in vertical subbands. A cross shaped window made of two oblique ellipses are employed in diagonal subbands because the energy clusters in this band are distributed approximately in the diagonal and antidiagonal directions. A cross shaped window is expressed as [41]:

$$W_{LD_d}(s_i, s_h) = \left\{(u,v) : \min\left\{s_h^4 p_w^2 + q_w^2, s_h^4 q_w^2 + p_w^2\right\} \leq s_h^2 s_i^2\right\} \quad (12)$$

where $(p_w, q_w) = (u - v, u + v)$ and $s_h > 1$. Fig. 4(a), 4(b) and 4(c) shows example of directional windows $W_{LD}(3, 2)$, $W_{LD}(3, 1/2)$ and $W_{LD_d}(3, 2)$ respectively and Fig. 5(a), 5(b) and 5(c) shows windows $W_{LD}(6, 2)$, $W_{LD}(6, 1/2)$ and $W_{LD_d}(6, 2)$ respectively.

The selection of shape and size of the elliptic directional window is very important in the proposed framework. Since
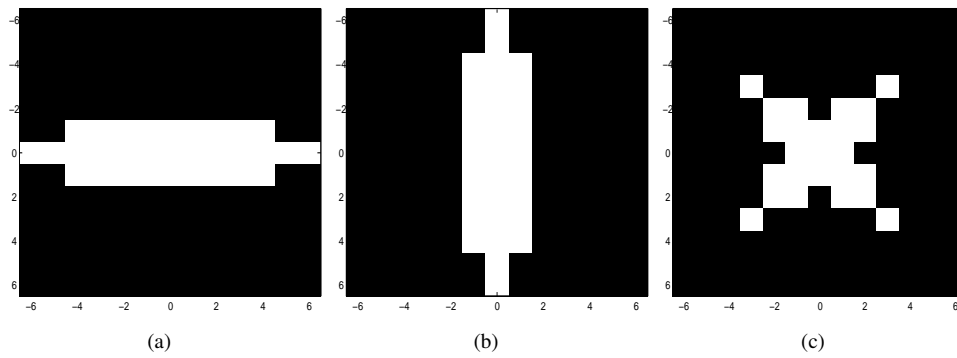
Fig. 4. Elliptic directional windows with s_i=3 and s_h=2 (a) Horizontal window (b) Vertical window and (c) Diagonal window
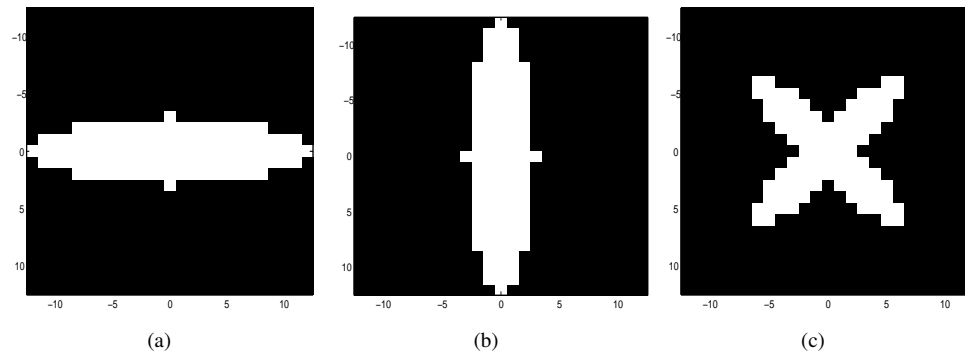

Fig. 5. Elliptic directional windows with s_i=6 and s_h=2 (a) Horizontal window (b) Vertical window and (c) Diagonal window

from the finest scale to coarsest scale the energy clusters reduces in size, the window sizes should also be reduced slowly from finest scale to the coarsest scale. The large window sizes should be used in high noise conditions and relatively smaller sized windows should be used in low noise cases[41]. The noise standard deviation is obtained from the noisy LOT coefficients in the first scale using [52]:

$$\hat{\sigma}_n = K_s \frac{Median\left(|z(i,j)|\right)}{0.6745}, z(i,j) \in HH_1 \qquad (13)$$

where K_s is a smoothing factor.

The second important step is the estimation of signal LOT coefficients using LMMSE estimator which is expressed as [38], [41]:

$$\hat{y}(m,n) = \frac{\hat{\sigma}_y^2(m,n)}{\hat{\sigma}_y^2(m,n) + \hat{\sigma}_n^2(m,n)} z(m,n) \qquad (14)$$

where $z(m,n)$ is the LOT coefficient of log-transformed SAR image.

The various steps involved in despeckling an SAR image using single LOT domain local Wiener filtering procedure are summarized as follows:

1) Apply the logarithm transformation on the SAR image
2) Perform block LOT operation on the log transformed SAR image
3) Arrange block LOT coefficients into octave-like form
4) Estimate signal variance using (10)
5) Estimate signal LOT coefficients using (14)
6) Rearrange LOT coefficients into block decomposition form
7) Perform inverse LOT operation on the coefficients obtained in step 6
8) The mean of log transformed noise is subtracted from the output obtained in step 7 [48], [43]

TABLE II
PSNR PERFORMANCE FOR DIFFERENT COMBINATIONS OF M USED IN LOCAL WIENER FILTER-1 PROCEDURE AND LOCAL WIENER FILTER-2 PROCEDURE FOR AN ARTIFICIALLY SPECKLED (L=4) 'AERIAL' IMAGE CORRESPONDING TO DLWF-LOT ALGORITHM

LOT-1	LOT-2	PSNR
M=4	M=8	22.42
M=8	M=8	22.14
M=16	M=8	22.32
M=4	M=16	**22.58**
M=8	M=16	22.46
M=16	M=16	22.27

9) Perform exponential operation on the values obtained in step 8

It has been shown in literature that the performance of single point Wiener filtering can be improved further by using empirical Wiener filtering which employs *pilot* signal [38], [41]. In this paper, we introduce a LOT domain dual local Wiener filtering structure (in homomorphic framework) to despeckle SAR images. Fig.6 shows the block diagram of proposed LOT domain framework. The framework uses two local Wiener filtering procedures where the first local Wiener filtering is performed in LOT-1 domain and uses (14) to produce an approximately clean version of the image which is used as a *pilot* image in the second local Wiener filtering procedure. The second LOT domain local Wiener filtering procedure makes use of the following equation to restore the noisy LOT coefficients:

$$\hat{y}_2(m,n) = \frac{\hat{\sigma}_{yp}^2(m,n)}{\hat{\sigma}_{yp}^2(m,n) + \hat{\sigma}_n^2(m,n)} z_{LOT-2}(m,n) \qquad (15)$$

where $z_{LOT-2}(m,n)$ is the coefficient of actual log-transformed SAR image in LOT-2 domain and $\sigma_{yp}^2(m,n)$ is
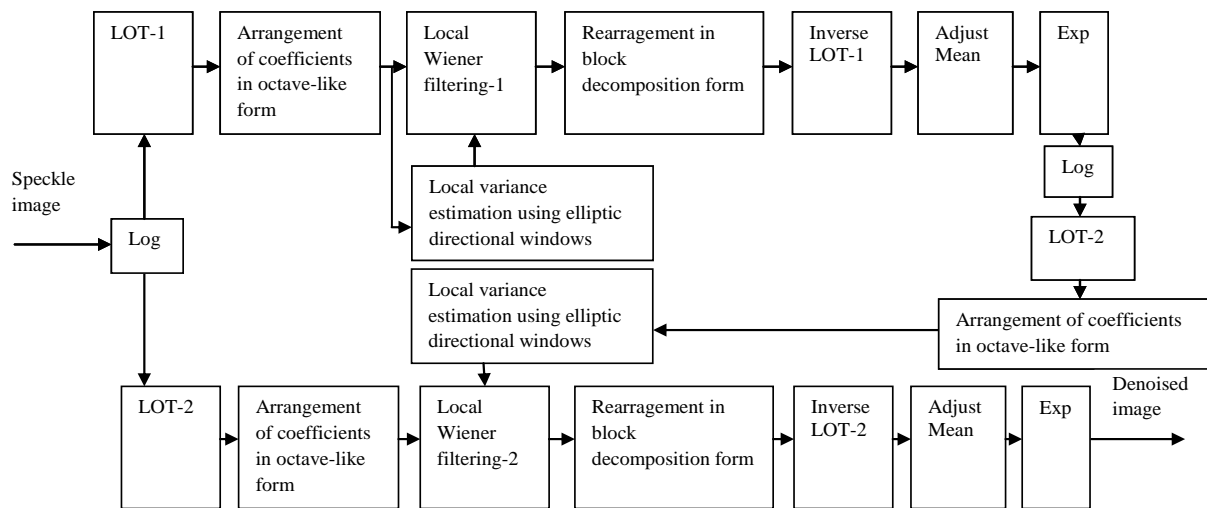
Fig. 6.   Block diagram of the proposed despeckling framework

the signal variance estimated from the *pilot* image in LOT-2 domain.

In [37], [41], [42], the authors demonstrated that the denoising performance can be improved further if two different wavelet bases are used in the empirical Wiener filtering structure. Since the application of LOT(M=4), LOT(M=8) and LOT(M=16) show quite different objective and subjective output results, we study the effect of employing five different combinations of M in first local Wiener filtering procedure and second local Wiener filtering procedure, on the despeckling performance (in terms of PSNR) of DLWF-LOT framework, for an artificially speckled 'aerial' image as shown in Table II. Table II demonstrates that the combination of LOT-1 with M=4 (first local Wiener filtering procedure) and LOT-2 with M=16 (second local Wiener filtering procedure) is the best combination and hence employed in the proposed DLWF-LOT structure.

IV. EXPERIMENTAL RESULTS

This section presents the despeckling results of proposed LOT based framework using synthetically speckled and real SAR images. We compare the performance of proposed method with three following well known despeckling techniques:

1) Linear MMSE filtering in undecimated wavelet transform domain [18]
2) PPB (iterative version) based method [6]
3) Directionlet based method [28]

The method discussed in [18], [6], [28], single LOT domain local Wiener filtering procedure for SAR image despeckling and proposed dual local Wiener filtering framework are referred to as UDWT-LMMSE, PPB, Directionlet, LWF-LOT and DLWF-LOT techniques respectively.

In the first local Wiener filtering procedure of DLWF-LOT, the elliptic directional windows $W_{LD}(s_i, s_h)$, $W_{LD}(s_i, 1/s_h)$ and $W_{LD_D}(s_i, s_h)$ with s_h=2, s_i=6 and 3, from finest to coarsest scale are used, respectively (large size windows should be used in high noise cases). In the second local Wiener filtering procedure of DLWF-LOT, we use s_h=2, s_i=2, 2, 1 and 1 from finest to coarsest scale,

respectively (relatively small size windows should be used in low noise cases). In LWF-LOT method, we perform LOT with M=16 and use the elliptic directional windows $W_{LD}(s_i, s_h)$, $W_{LD}(s_i, 1/s_h)$ and $W_{LD_D}(s_i, s_h)$ with s_h=2, s_i=8, 4, 2, 2 from finest to coarsest scale are used, respectively. The UDWT-LMMSE implementation uses four multiresolution levels and 9/7 biorthogonal wavelet. The results of PPB method have been obtained using publically available Matlab code made available by its authors on their website. The results were obtained using 25 number of iterations, T=0.2, α=0.92, 21x21 search window with 7x7 patch. The results of UDWT-LMMSE scheme have been obtained from the authors through direct web based service and the results of directionlet based method have been obtained using authors own code run by the authors themselves on our SAR images.

A. With synthetically speckled Aerial images

The use of synthetically speckled aerial images, with its noise free version available, allows objective performance analysis. The aerial images resembles real SAR images in terms of very similar scene features. The original aerial images used in this subsection are shown in Fig. 7. The aerial
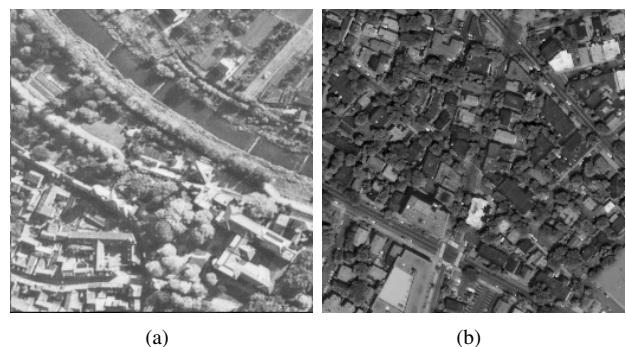

(a)   (b)

Fig. 7.   Original aerial images used in experiments (a) 'Aerial1' image (256x256) (b) 'Aerial2' image (256x256)

image 'Aerial1' shown in Fig. 7(a) is obtained from USC-SIPI image database (www.sipi.usc.edu/database/). The aerial image 'Aerial2' shown in Fig. 7(b) is obtained by cropping

'boston' image available in Matlab's image processing tool-box. Three different levels of artificially generated speckle noise with L=2, 4 and 16 are used in the simulation.

In the LWF-LOT implementation, for synthetically speckled and real SAR images, the value of K_s is set to 1. In the DLWF-LOT implementation, for synthetically speckled images, the value of K_s is set to 0.88 and 1 in the local Wiener filtering-1 and local Wiener filtering-2 procedures respectively.

Three widely used objective metrics are employed for despeckling performance comparison:

1) Signal to mean square error (S/MSE) ratio
2) Structural similarity (SSIM) index
3) Edge preservation index (β)

The $\frac{S}{MSE}$ ratio in decibels is defined as [53]

$$\frac{S}{MSE} = 10 \log_{10} \left(\frac{\sum\limits_{i=1}^{N} Y_i^2}{\sum\limits_{i=1}^{N} (\hat{Y}_i - Y_i)^2} \right) \qquad (16)$$

where N denotes size of the image and Y and $\hat{Y}$ are noise free and despeckled images respectively. The SSIM index [54] measures the structural similarity between the noise free version of the image and its distorted form (in this case, the despeckled image). SSIM index is a good indicator of perceived image quality and popularly used in the literature for comparing the denoising performance of different techniques. The publicly available Matlab code (www.ece.uwaterloo.ca/ z70wang/research/ssim) is used for calculating the SSIM index. The edge preservation index (β) is used to evaluate the performance of edge preservation and is computed using the following expression [16]:

$$\beta = \frac{\Gamma\left(\Delta Y - \overline{\Delta Y}, \widehat{\Delta Y} - \overline{\widehat{\Delta Y}}\right)}{\sqrt{\Gamma\left(\Delta Y - \overline{\Delta Y}, \Delta Y - \overline{\Delta Y}\right)\Gamma\left(\widehat{\Delta Y} - \overline{\widehat{\Delta Y}}, \widehat{\Delta Y} - \overline{\widehat{\Delta Y}}\right)}} \qquad (17)$$

where ΔY and $\widehat{\Delta Y}$ are the high pass filtered versions of noise free image and despeckled image respectively. By applying Laplacian of Gaussian (LOG) filter, the required high pass filtered version of the images were obtained. The $\overline{\Delta Y}$ and $\overline{\widehat{\Delta Y}}$ denotes the mean values of ΔY and $\widehat{\Delta Y}$ respectively and $\Gamma(a,b) = \sum\limits_{i,j} a(i,j)b(i,j)$. For optimal effect of edge preservation, the β should be close to one.

Table III shows that UDWT-LMMSE method performs best in terms of S/MSE ratio but exhibits low β values, compared to PPB and DLWF-LOT methods. PPB method outperforms UDWT-LMMSE and Directionlet method in terms of β value. The proposed LOT based framework provides larger values of edge preservation factor (β) and SSIM index results in comparison to all other methods, therefore indicating a better ability to preserve edge structures and provides despeckled images with better perceived image quality. Fig. 8 shows the visual results for 'Aerial2' image. The despeckled image provided by Directionlet method shows oversmoothing of important details (Fig 8(d)). Fig. 8(b) demonstrates that UDWT-LMMSE method is well efficient in reducing the speckle but shows slightly inferior results in retaining the edges compared to PPB and proposed method. The proposed method when compared to UDWT-LMMSE,

PPB, Directionlet and LWF-LOT methods (Fig.8(b), 8(c) and 8(d)) shows good trade off between smoothing and texture preservation.

B. Using real SAR images

The despeckling performance assessment in SAR image despeckling, in the absence of clean images, is a very tough task. Out of various performance measures available in literature we have used the following widely popular measures:

1) Equivalent number of looks (ENL): ENL represents the degree of speckle smoothing in a homogeneous region. Higher ENL value indicates better speckle reduction. Theoretically, the ENL value equals the number of looks of an intensity image. It is computed as [19], [17], [25]:

$$ENL = \frac{E\{\widehat{Y_{SAR}}\}^2}{\text{var}\{\widehat{Y_{SAR}}\}} \qquad (18)$$

where $E\{\widehat{Y_{SAR}}\}$ and $\text{var}\{\widehat{Y_{SAR}}\}$ are estimated from a homogeneous region in the despeckled image.

2) Edge save index (ESI): ESI [55], [56], [28] indicates the edge preservation ability of the despeckling method. The ESI is computed in the horizontal (ESI^H) and vertical (ESI^V) directions. The ESI^H is computed from the following expression

$$ESI^H = \frac{\sum\limits_{i=1}^{r}\sum\limits_{j=1}^{c-1}\left|\hat{Y}_{SAR}(i,j+1) - \hat{Y}_{SAR}(i,j)\right|}{\sum\limits_{i=1}^{r}\sum\limits_{j=1}^{c-1}\left|Z_{SAR}(i,j+1) - Z_{SAR}(i,j)\right|}$$
$$(19)$$

where $\hat{Y}_{SAR}$ is despeckled image and Z_{SAR} is the original SAR image. r and c denotes the number of of rows and columns in the SAR image. The ESI^V is computed from the following expression

$$ESI^V = \frac{\sum\limits_{j=1}^{c}\sum\limits_{i=1}^{r-1}\left|\hat{Y}_{SAR}(i+1,j) - \hat{Y}_{SAR}(i,j)\right|}{\sum\limits_{j=1}^{c}\sum\limits_{i=1}^{r-1}\left|Z_{SAR}(i+1,j) - Z_{SAR}(i,j)\right|}$$
$$(20)$$

The higher the ESI, the better the edge saving ability.

3) Ratio image analysis: Ratio image [57], [58], [59] is the pointwise ratio of real SAR image to the despeckled image. In case of ideal despeckling, the ratio image should contain speckle only.

   a) Ratio image mean (M_{RI}): M_{RI} indicates the degree of radiometric preservation and is ideally equals to one. Hence, despeckling methods which provide M_{RI} close to unity indicate better performance of radiometric preservation.

   b) Visual analysis of ratio image: The visual analysis of ratio image also indicates the performance of a despeckling technique. The presence of any structural details correlated to the actual image shows that the despeckling technique has smoothened not only speckle noise but few important details also.

TABLE III
S/MSE, SSIM AND β VALUES OBTAINED BY DIFFERENT DESPECKLING ALGORITHMS FOR TWO AERIAL IMAGES

| | 'Aerial1' | | | | | | | | |
| | L=2 | | | L=4 | | | L=16 | | |
	S/MSE	SSIM	β	S/MSE	SSIM	β	S/MSE	SSIM	β
UDWT-LMMSE	**16.26**	0.6325	0.3451	17.92	0.7394	0.4693	21.84	0.8824	0.7163
It. PPB	16.34	0.5808	0.3469	**18.26**	0.7279	**0.5090**	21.07	0.8691	0.6980
Directionlet	13.38	0.5508	0.3313	16.49	0.6945	0.4564	20.89	0.8451	0.6909
LWF-LOT	14.27	**0.6625**	0.3530	17.52	0.7610	0.4848	21.86	0.8830	0.7361
DLWF-LOT	14.01	0.6610	**0.3671**	17.49	**0.7667**	0.4975	**21.94**	**0.8860**	**0.7408**
	'Aerial2'								
	L=2			L=4			L=16		
	S/MSE	SSIM	β	S/MSE	SSIM	β	S/MSE	SSIM	β
UDWT-LMMSE	**13.97**	0.6877	0.3907	**15.61**	0.7865	0.5364	**19.71**	**0.9149**	0.7458
It. PPB	13.87	0.6673	0.4334	15.10	0.7711	0.5500	17.49	0.8666	0.6706
Directionlet	12.01	0.6181	0.4004	14.59	0.7446	0.5568	18.09	0.8637	0.7317
LWF-LOT	12.62	0.7223	0.4297	15.38	0.8080	0.5901	18.92	0.8972	0.7585
DLWF-LOT	12.35	**0.7248**	**0.4365**	15.29	**0.8132**	**0.5985**	19.49	0.9100	**0.7677**

(a)   (b)   (c)

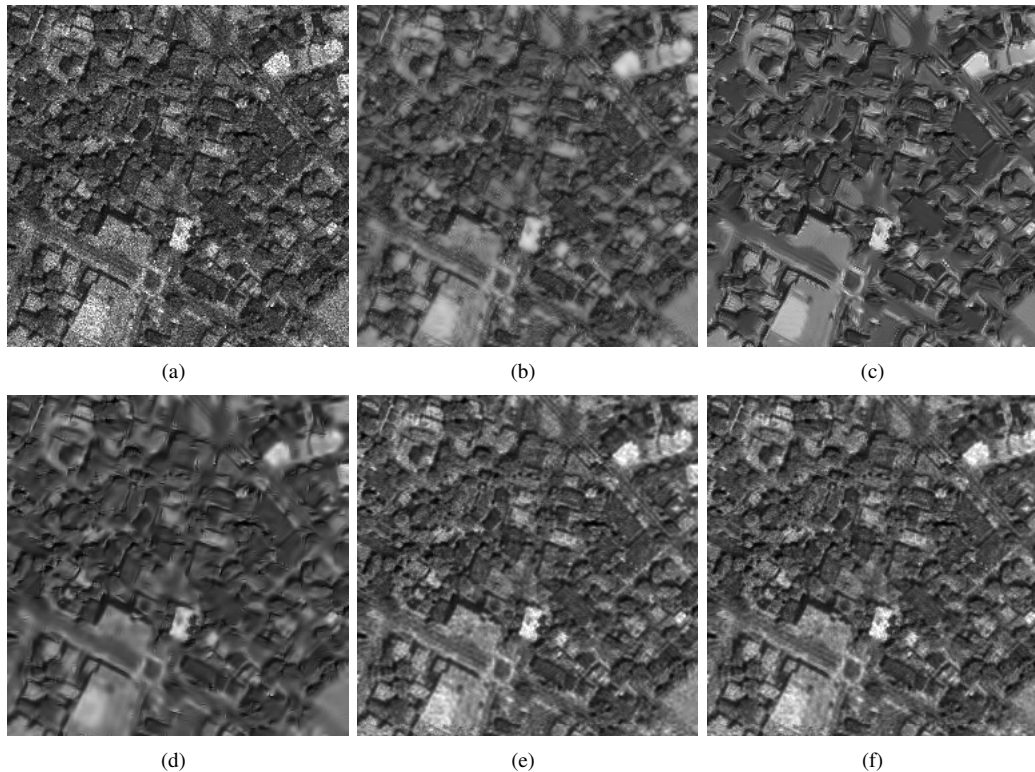(d)   (e)   (f)

Fig. 8.   Despeckled images for 'Aerial2' image (a) Noisy (L=4) (b) Using UDWT-LMMSE [18] (c) Using It. PPB [6] (d) Using Directionlet [28] (e) Using LWF-LOT (f) Using DLWF-LOT

In this paper, we report the experimental results for three real SAR images (displayed in Fig. 9). The real SAR images used for various experiments in this paper are freely available for download at www.sandia.gov/RADAR/sar.html. Fig.9(a), 9(c) are Ku-band SAR images and Fig. 9(b) is a X-band SAR image acquired by twin otter aircraft of Sandia National Laboratories. Fig. 9(a) shows an intensity image of Horsetrack near Albuquerque, New Mexico, Fig. 9(b) shows an intensity image of Hangars at Kirtland AFB, Albuquerque, New Mexico and Fig. 9(c)shows an intensity image of sports complex, Albuquerque, New Mexico.

In the DLWF-LOT implementation, for real SAR images, the value of K_s is set to 1.1 and 1 in the local Wiener filtering-1 and local Wiener filtering-2 procedures respectively.

The ENL and ESI values obtained for various despeckling methods are provided in Table IV. For ENL computation two homogeneous regions, 'Region1' and 'Region2', in

each SAR image have been selected. Region1 and Region2 comprise of 30x43 and 40x35 pixels in 'horsetrack', 25x43 and 37x21 pixels in 'stadium' and 12x33 and 20x30 pixels in 'hangars' respectively. It is obvious from Table IV that the DLWF-LOT method outperforms the UDWT-LMMSE method and PPB method both in terms of ENL and ESI values in most of the situations. The directionlet based method provides very high value of ENL compared to all other methods including proposed method, which is achieved at the cost of oversmoothed images, the same can be verified by observing extremely low values of ESI. The UDWT-LMMSE method exhibits very low values of ESI compared to PPB and DLWF-LOT methods.

As shown in Table V, the LOT based methods in most of the cases, obtains closer results to the ideal value of M_{RI} which indicates its better ability of radiometric preservation.

The despeckled images obtained from UDWT-LMMSE, PPB, directionlet based method, LWF-LOT and DLWF-LOT
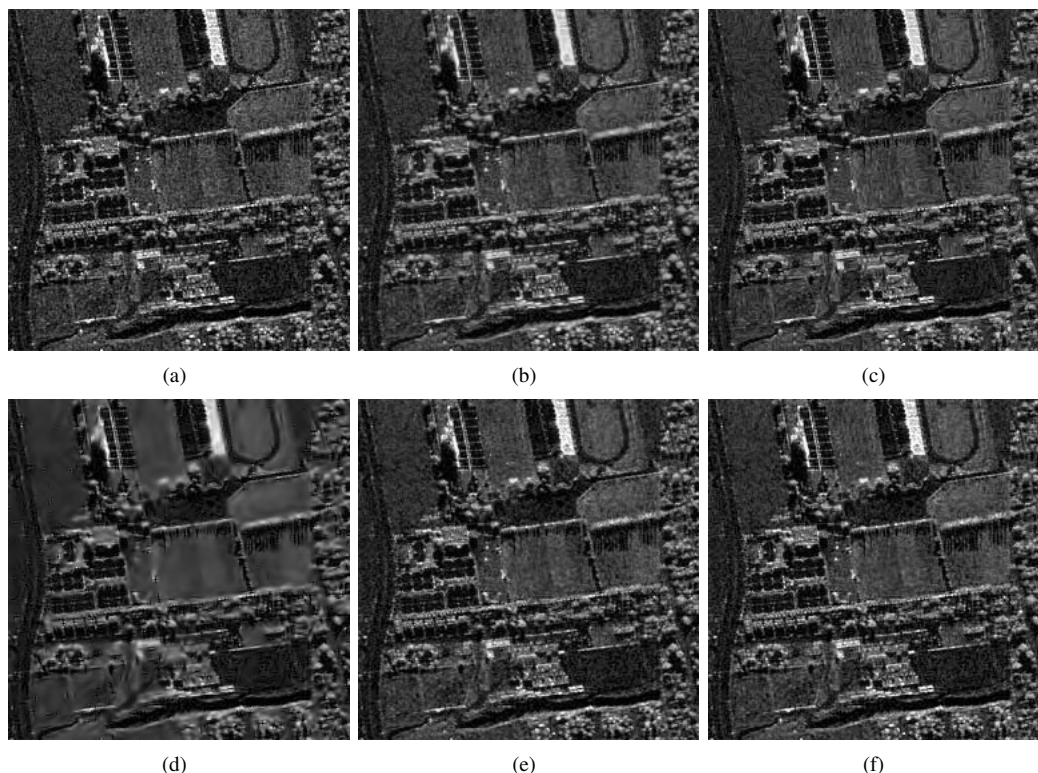
Fig. 10. Despeckled images for 'stadium' SAR image (a) Original image (b) Using UDWT-LMMSE [18] (c) Using PPB [6] (d) Using Directionlet [28] (e) Using LWF-LOT (f) Using DLWF-LOT
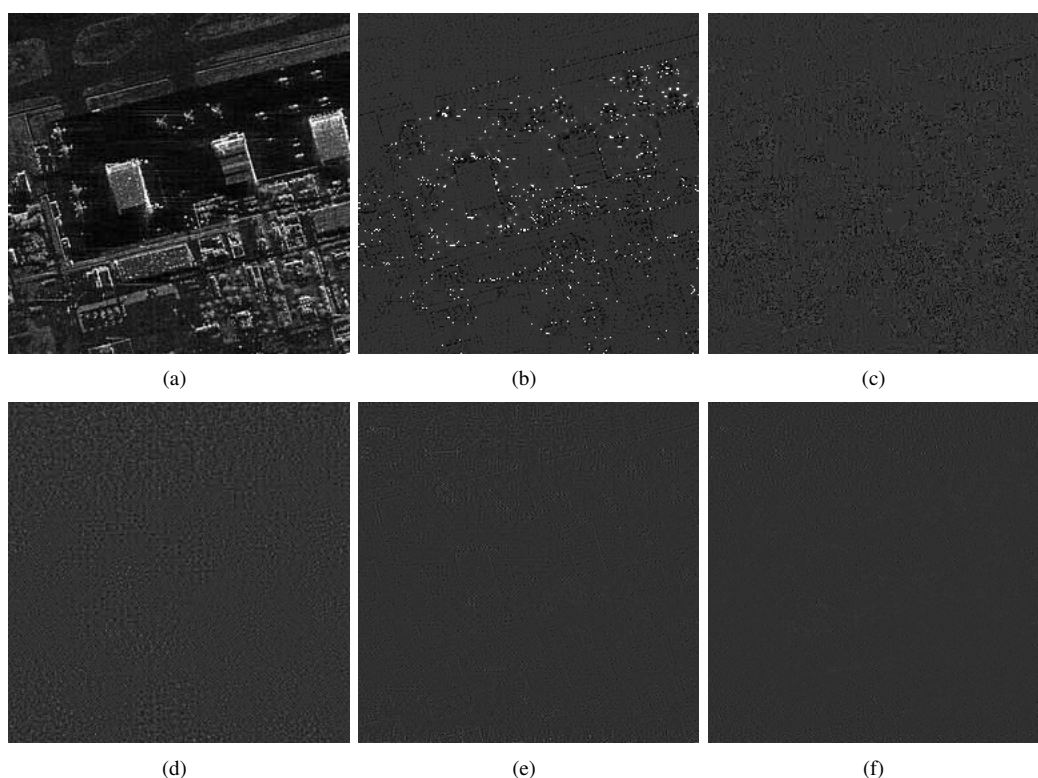

Fig. 11. Ratio images for 'hangars' (a) Original image (b) Using UDWT-LMMSE [18] (c) Using PPB [6] (d) Using Directionlet [28] (e) Using LWF-LOT (f) Using DLWF-LOT

methods are shown in Fig. 10. It is observed that the speckle noise is well reduced in almost all the despeckled images, however in terms of details and edge preservation the DLWF-LOT method performs the best. The output image (Fig. 10(d)) obtained using Directionlet method clearly shows oversmoothing of details.

The superiority of DLWF-LOT over UDWT-LMMSE, PPB, directionlet and LWF-LOT methods can also be verified by visual inspection of ratio images shown in Fig. 11. The ratio images shown in Fig. 11(b), 11(c), 11(d) and 11(e)
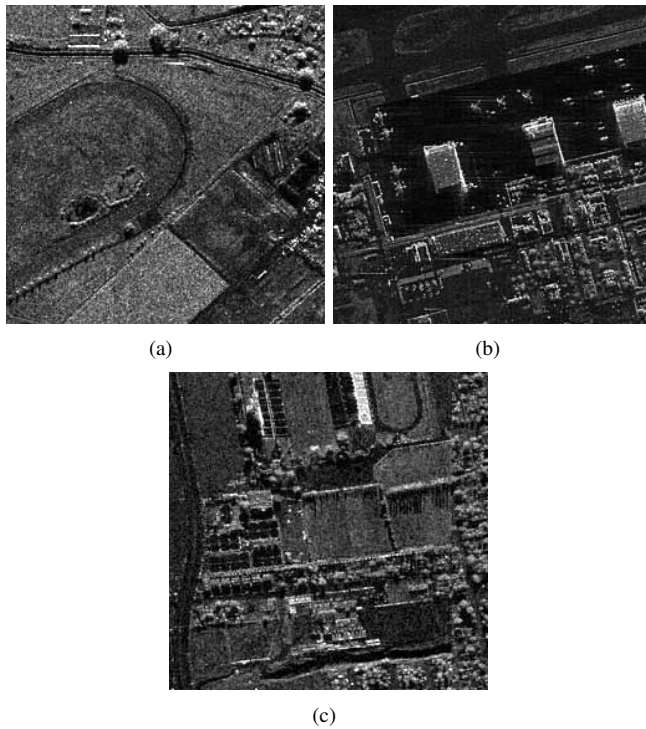
(a)   (b)

(c)

Fig. 9. Three real SAR images used in the experiments (a) 'horsetrack'(b) 'hangars' (c) 'stadium'.(Image Courtesy of Sandia National Laboratories, Airborne ISR)

TABLE IV
ENL AND ESI VALUES OBTAINED BY DIFFERENT DESPECKLING ALGORITHMS FOR THREE REAL SAR IMAGES

	'horsetrack'			
	ENL		ESI	
	Region1	Region2	ESI^H	ESI^V
Original	15.57	11.43	–	–
UDWT-LMMSE	32.52	22.49	0.6714	0.7268
PPB	36.01	18.77	0.7435	0.8048
Directionlet	**666.62**	**69.92**	0.3626	0.4436
LWF-LOT	55.35	23.62	0.7290	0.7804
DLWF-LOT	50.68	21.17	**0.7856**	**0.8312**
	'stadium'			
	ENL		ESI	
	Region1	Region2	ESI^H	ESI^V
Original	14.92	21.79	–	–
UDWT-LMMSE	25.59	36.99	0.8294	0.8600
PPB	21.87	33.92	0.8440	0.8715
Directionlet	**123.62**	**133.91**	0.5468	0.5971
LWF-LOT	29.42	43.13	0.8221	0.8496
DLWF-LOT	28.45	37.96	**0.8925**	**0.9116**
	'hangars'			
	ENL		ESI	
	Region1	Region2	ESI^H	ESI^V
Original	12.35	11.18	–	–
UDWT-LMMSE	20.26	17.08	0.7770	0.8228
PPB	17.70	14.83	0.7869	0.8539
Directionlet	**48.22**	**28.12**	0.7056	0.7605
LWF-LOT	23.50	24.13	0.8691	0.9062
DLWF-LOT	18.44	17.44	**0.9412**	**0.9681**

clearly shows presence of some edge structures and patterns which indicates that these techniques not only removes noise but some important informations also. Fig. 11(f) provides least structural details from original image. The visual results on real SAR images seems to be consistent with the results reported in Table IV.

TABLE V
M_{RI} VALUES OBTAINED BY DIFFERENT DESPECKLING ALGORITHMS FOR THREE REAL SAR IMAGES

	Mean of ratio image (M_{RI})		
	'horsetrack'	'stadium'	'hangars'
UDWT-LMMSE	0.9683	0.9707	0.9905
PPB	0.9712	0.9739	0.9729
Directionlet	1.0366	1.0500	1.0179
LWF-LOT	0.9791	0.9868	0.9679
DLWF-LOT	0.9760	0.9789	0.9657

V. CONCLUSION

An effective LOT domain dual local Wiener filtering framework is proposed for SAR image despeckling. It was shown that Gaussian distribution is able to model the local statistics of dyadic rearranged LOT coefficients of the logarithmically transformed reflectance image. Experimental results show that the proposed despeckling method outperforms several recent well known methods and can achieve both the speckle reduction and texture preservation simultaneously with much less computational complexity.

REFERENCES

[1] J. Lee, "Digital image enhancement and noise filtering by use of local statistics," *IEEE Transactions Pattern Analysis Machine Intelligence*, vol. Vol. PAMI-2, no. 2, pp. 165–168, 1980.
[2] K. S. V. Frost, J. Stiles and J. Holtzman, "A model for radar images and its application to adaptive digital filtering of multiplicative noise," *IEEE Transactions Pattern Analysis Machine Intelligence*, vol. PAMI-4, no. 2, pp. 157–166, 1982.
[3] T. S. D. Kuan, A. Sawchuk and P. Chavel, "Adaptive restoration of images with speckle," *IEEE Transactions Accost., Speech, Signal processing*, vol. ASSP-35, no. 3, pp. 373–383, 1987.
[4] A. Baraldi and F. Parmigiani, "A refined gamma map sar speckle filter with improved geometrical adaptivity," *IEEE Transactions on Geoscience and Remote Sensing*, vol. 33, pp. 1245–1257, 1995.
[5] Y. Yu and S. T. Acton, "Speckle reducing anisotropic diffusion," *IEEE Trans. Image Processing*, vol. 11, no. 11, pp. 1260–1270, 2002.
[6] C. A. Deledalle, L. Denis, and F. Tupin, "Iter. weighted max. likelihod denoising with probabilistic patch-based weights," *IEEE Trans. on Image Process.*, vol. 18, no. 12, pp. 1–12, 2009.
[7] D. P. K. Lun and W. C. Siu, "A deblocking technique for block-transform compressed image using wavelet transform modulus maxima," *IEEE Trans. Image Processing*, vol. 7, pp. 1488–1496, 1998.
[8] S. Chang, B. Yu, and M. Vetterli, "Adaptive wavelet thresholding for image denoising and compression," *IEEE Transactions on Image Processing,*, vol. 9, pp. 1532–1546, 2000.
[9] J. Cheng, Y. Liu, R. Jia, and W. Guo, "A new active contour model for medical image analysis-wavelet vector flow," *IAENG International Journal of Applied Mathematics*, vol. 36, no. 2, pp. 33–37, 2007.
[10] L. W. Chew, W. C. Chia, L. minn Ang, and K. P. Seng, "An optimum approach for image compression: Tuned degree-k zerotree wavelet coding," *IAENG International Journal of Computer Science*, vol. 36, no. 2, pp. 175–182, 2009.
[11] K. H. Talukder and K. Harada, "Haar wavelet based approach for image compression and quality assessment of compressed image," *IAENG International Journal of Applied Mathematics*, vol. 36, no. 1, pp. 49–56, 2007.
[12] G. Wan, X. Song, and R. Bettati, "An improved ezw algorithm and its applications in intelligent transportation systems," *Engineering Letters*, vol. 22, no. 2, pp. 63–69, 2014.
[13] K. H. Talukder and K. Harada, "Use of concurrent wavelet transform (wt) to image compression and a verification analysis of communicating threads for concurrent wt," *Engineering Letters*, vol. 16, no. 2, pp. 202–209, 2008.
[14] L. Ma, J. Ma, and Y. Shen, "Pixel fusion based curvelets and wavelets denoise algorithm," *Engineering Letters*, vol. 14, no. 2, pp. 130–134, 2007.
[15] J. R. Sveinsson and J. A. Benediktsson, "Speckle reduction and enhancement of sar images in the wavelet domain," in *IGARSS*, 1996.
[16] A. Achim, P. Tsakalides, and A. Bezarianos, "Sar image denoising via bayesian wavelet shrinkage based on heavy tail modeling," *IEEE Transactions on Geoscience Remote Sensing*, vol. 41, no. 8, pp. 1773–1784, 2003.

[17] M. I. H. Bhuiyan, M. O. Ahmad, and M. N. S. Swamy, "Spatially adaptive wavelet-based method using the cauchy prior for denoising the sar images," *IEEE Transactions on Circuits and Systems for Video Technology*, vol. 17, no. 4, pp. 500 – 507, 2007.

[18] F. Argenti and L. Alparone, "Speckle removal from sar images in the undecimated wavelet domain," *IEEE Transactions on Geoscience and Remote sensing*, vol. 40, no. 11, pp. 2363–2374, 2002.

[19] S. Solbo and T. Eltoft, "Homomorphic wavelet based statistical despeckling of sar images," *IEEE Transactions on Geoscience and Remote Sensing*, vol. 42, no. 4, pp. 711–721, 2004.

[20] A. K. Jain, *Fundamentals of digital image processing*. Prentice Hall, 1989.

[21] S. Solbo and T. Eltoft, "Gamma-wmap: A statistical speckle filter operating in the wavelet domain," *International Journal of Remote Sensing*, vol. 25, no. 5, pp. 1019–1036, 2004.

[22] M. Amirmazlaghani and H. Amindavar, "A novel wavelet domain statistical approach for denoising sar images," in *International conference on Image Processing (ICIP)*, 2009, pp. 3861–3864.

[23] F. Argenti, T. Bianchi, and Luciano, "Multiresolution map despeckling of sar images based on locally adaptive generalized gaussian pdf modeling," *IEEE Transactions on Image Processing*, vol. 15, no. 11, pp. 3385–3399, 2006.

[24] F. Argenti, T. Bianchi, and L. Alparone, "Fast map despeckling based on laplacian-gaussian modeling of wavelet coefficients," *IEEE Geoscience and Remote Sensing Letters*, vol. 9, no. 1, pp. 13–17, 2012.

[25] S. Parrilli, M. Poderico, C. V. Angelino, and L. Verdoliva, "A nonlocal sar image denoising algorithm based on llmmse wavelet shrinkage," *IEEE Transactions on Geoscience and Remote Sensing*, vol. 50, no. 2, pp. 606–616, 2012.

[26] B. Hou, X. Zhang, X. Bu, and H. Feng, "Sar image despeckling based on nonsubsampled shearlet transform," *IEEE Journal of selected topics in applied earth observations and remote sensing*, vol. 5, no. 3, pp. 809–823, 2012.

[27] F. Argenti, T. Bianchi, G. M. di Scarfizzi, and L. Alparone, "Lmmse and map estimators for reduction of multiplicative noise in the nonsubsampled contourlet domain," *Signal Processing*, vol. 89, pp. 1891–1901, 2009.

[28] R. Sethunadh and T. Thomas, "Sar image despeckling in directionlet domain based on edge detection," *IEE Electr. Letters*, vol. 49, no. 6, pp. 422 – 424, 2013.

[29] V. K. Nath, "Statistical modeling of lapped transform coefficients and its applications," Ph.D. dissertation, Indian Institute of Technology Guwahati (IITG), Deptt. of Electronics and Electrical Engineering, 2011.

[30] L. Duval and T. Q. Nguyen, "Lapped transform domain denoising using hidden markov trees," in *IEEE ICIP*, vol. 1, 2003, pp. 125–128.

[31] B. S. Raghvendra and P. S. Bhat, "Image denosing using mixture distributions with lapped transforms," in *National Conference of Communications*, 2006, pp. 217–220.

[32] V. K. Nath, D. Hazarika, and A. Mahanta, "Lapped transform-based image denoising with the generalized gaussian prior," *International Journal of Comput. Vision and Robotics*, vol. 4, no. 1/2, pp. 55–74, 2014.

[33] L. Duval and T. Q. Nguyen, "Hidden markov tree image denoising with redundant lapped transforms," in *IEEE International Conference on Acoustics, Speech and Signal Processing*, vol. 3, 2004, pp. 193–196.

[34] D. Hazarika and M. Bhuyan, "Despeckling sar images in the lapped transform domain," in *National Conference on Computer Vision, Pattern Recognition, Image processing and Graphics (NCVPRIPG)*. IEEE, 2013, pp. 1–5.

[35] H. S. Malvar, "The lot : Transform coding without blocking effects," *IEEE Trans. on Acc., Speech and Signal Process.*, vol. 37, no. 4, pp. 553–559, 1989.

[36] ——, "Fast progressive image coding without wavelets," in *Data Comp. Conf.*, 2000, pp. 243–252.

[37] S. P. Ghael, A. M. Sayeed, and R. G. Baraniuk, "Improved wavelet denoising via empirical wiener filtering," *SPIE*, pp. 389–399, 1997.

[38] M. K. Michak, I. Kozintsev, and K. Ramchandran, "Low complexity image denoising based on statistical modelling of wavelet coefficient," *IEEE Signal Processing Letters*, vol. 6, no. 12, pp. 300–303, 1999.

[39] M. Kazubek, "Wavelet domain image denoising by thresholding and wiener filtering," *IEEE Signal Processing Letters*, vol. 10, no. 11, pp. 324–326, 2003.

[40] I. K. Eom and Y. S. Kim, "Wavelet-based denoising with nearly arbitrarily shaped windows," *IEEE Signal Processing Letters*, vol. 11, no. 12, pp. 937–940, 2004.

[41] P.-L. Shui, "Image denoising algorithm via doubly local wiener filtering with directional windows in wavelet domain," *IEEE Signal Process. Letters*, vol. 12, no. 10, pp. 681–684, 2005.

[42] P. lang Shui and Y.-B. Zhao, "Image denoising algorithm using doubly local wiener filtering with block adaptive windows in wavelet domain," *Signal Processing*, vol. 87, pp. 1721–1734, 2007.

[43] M. I. H. Bhuiyan, M. O. Ahmad, and M. N. S. Swamy, "Wavelet-based image denoising with the normal inverse gaussian prior and linear mmse estimator," *IET Image Processing*, vol. 2, no. 4, pp. 203–217, 2008.

[44] H. S. Malvar, *Signal Processing with Lapped Transforms*. Norwood, MA : Artech House, 1992.

[45] Z. Xiong, O. G. Guleryuz, and M. T. Orchard, "A dct based embedded image coder," *IEEE Signal Processing Letters*, vol. 3, no. 11, pp. 289–290, 1996.

[46] C. Oliver and S. Quegan, *Understanding Synthetic Aperture Radar Images*. Raleigh, NC: SciTech, 2004.

[47] J. Goodman, "Some fundamental properties of speckle," *Journal of the Optical Society of America*, vol. 66, no. 11, pp. 1145–1150, 1976.

[48] H. Xie, L. E. Pierce, and F. T. Ulaby, "Statistical properties of logarithmically transformed speckle," *IEEE Trans. on Geosc. and Remote Sensing*, vol. 40, no. 3, pp. 721–727, 2002.

[49] S. M. Kay, *Fundamentals of statistical signal processing: estimation theory*. Prentice-Hall Ltd, Englewood Cliffs, USA, 1993.

[50] M. K. Michak, I. Kozintsev, and K. Ramchandran, "Spatially adaptive statistical modeling of wavelet image coefficients and its application to denoising," in *IEEE International Conference on Accoustics, Speech and Signal Processing*, vol. 6, 1999, pp. 3253–3256.

[51] J. M. Park, W. J. Song, and W. A. Pearlman, "Speckle filtering of sar images based on adaptive windowing," in *Inst. Elect. Eng., Vis., Image Signal Processing*, vol. 146, no. 33, 1999, pp. 191–197.

[52] D. L. Donoho and I. M. Johnstone, "Ideal spatial adaptation by wavelet shrinkage," *Biometrika*, vol. 3, no. 81, pp. 425–455, 1994.

[53] L. Gagnon and A. Jouan, "Speckle filtering of sar images- a comparative study between complex wavelet based and standard filters," *Proc. SPIE*, 1997.

[54] Z. Wang, A. C. Bovik, H. R. Sheikh, and E. P. Simoncelli, "Image quality assessment : From error visibility to structural similarity," *IEEE Transactions on Image processing*, vol. 13, no. 4, pp. 600–612, 2004.

[55] W. G. Zhang, F. Liu, and L. C. Jiao, "Sar image despeckling via bilateral filtering," *IEE Electronics Letters*, vol. 45, no. 15, July 2009.

[56] W. G. Zhang, Q. Zhang, and C. S. Yang, "Improved bilateral filtering for sar image despeckling," *IEE Electronics Letters*, vol. 47, no. 4, 2011.

[57] D. Gleich and M. Datcu, "Wavelet-based sar image despeckling and information extraction, using particle filter," *IEEE Trans. on Image Process.*, vol. 18, no. 10, pp. 2167–2184, 2009.

[58] Q. Gao, Y. Lu, D. Sun, Z.-L. Sun, and D. Zhang, "Directionlet based de-noising of sar images using a cauchy model," *Signal Processing*, vol. 93, pp. 1056–1063, 2013.

[59] Y. Lu, Q. Gao, D. Sun, and D. Zhang, "Directionlet-based method using the gaussian mixture prior to sar image despeckling," *International journal of Remote Sensing*, vol. 35, no. 3, pp. 1143–1161, 2014.